Electronic Supplementary Information

Encapsulation of Au/Fe_3O_4 nanoparticles into polymer nanoarchitecture with combined near infrared-triggering chemo-photothermal therapy based on intracellular secondary protein understanding

Ching-Wen Chen,[a,⊥] Wei-Jhe Syu,[a,⊥] Tzu-Chi Huang,[b] Yao-Chang Lee,[c] Jong-Kai Hsiao,[d] Kuo-Yi Huang,[e] Hsiu-Ping Yu,[a] Mei-Yi Liao,[b*] and Ping-Shan Lai [a*]

[a] Department of Chemistry, National Chung Hsing University Taichung 402, Taiwan.
[b] Department of Applied Chemistry, National Pingtung University, Pingtung 90003, Taiwan.
[c] National Synchrotron Radiation Research Center, Hsinchu Science Park, Hsinchu 30076, Taiwan.
[d] Department of Medical Imaging Buddhist Tzu Chi General Hospital, Taipei Branch New Taipei City 231, Taiwan.
[e] Department of Bio-Industrial Mechatronics Engineering,, National Chung Hsing University Taichung 402, Taiwan.
[⊥] Dr. Ching-Wen Chen and Dr. Wei-Jhe Syu contributed equally to this work.
[*] E-mail: pslai@email.nchu.edu.tw

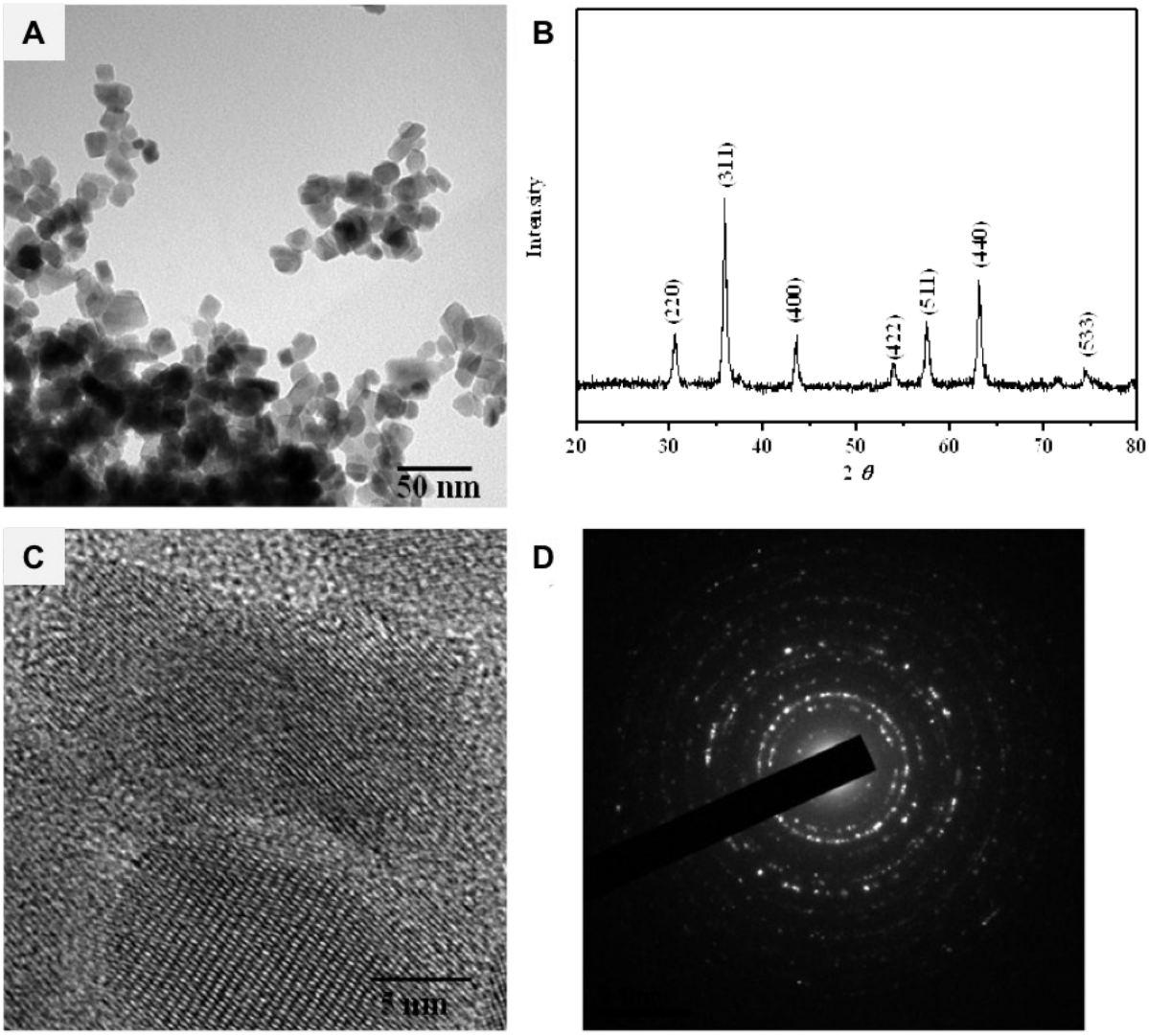

Fig. S1. A) TEM image, B) XRD pattern, C) HR-TEM image, and D) ED pattern of polyhedral Fe_3O_4 nanoparticles prepared using $FeCl_2$ + citrate + benzoic acid via a hydrothermal reaction at 200 °C for 12 h.

Intriguingly, we found that this polymer self-assembly reaction was very sensitive to the acid additive according to the corresponding photoabsorption of the Au@polymer NPs was increased in the NIR wavelength region after the addition of 18 μL of HCl (2 N), ascribing to the generation of numerous Au nanoparticle aggregates within PSMA polymer spheres (Fig. S2B). The particles grew to bigger spherical shapes (~320 nm) with the optical

absorption band in the NIR wavelength region increased (Fig. S2C) compared to a single peak at ~ 545 nm of the single-domain Au@polymer NPs (~74 nm).

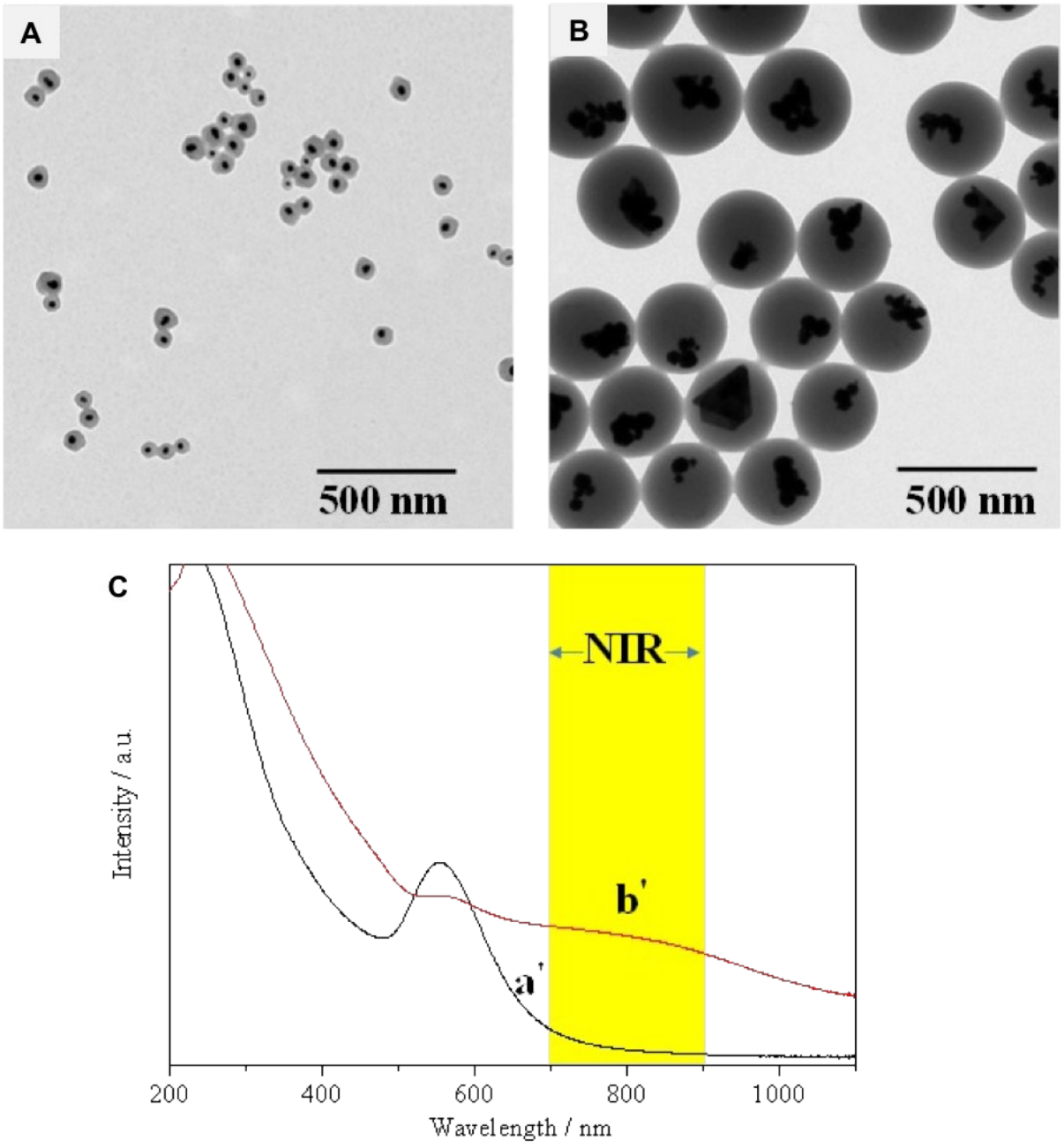

Fig. S2. TEM images of Au@polymer nanoparticles from the reaction of A) 1 mL of $HAuCl_4$ (5 mM) with 10 mL of PSMA (6 mg/mL) and B) 1 mL of $HAuCl_4$ (5 mM) with 10 mL of PSMA (6 mg/mL) with 18 μL of HCl (2 M) after 13 h of hydrothermal reaction. C) UV-visible spectra of the Au@polymer from A) and B), labeled as a' and b'.

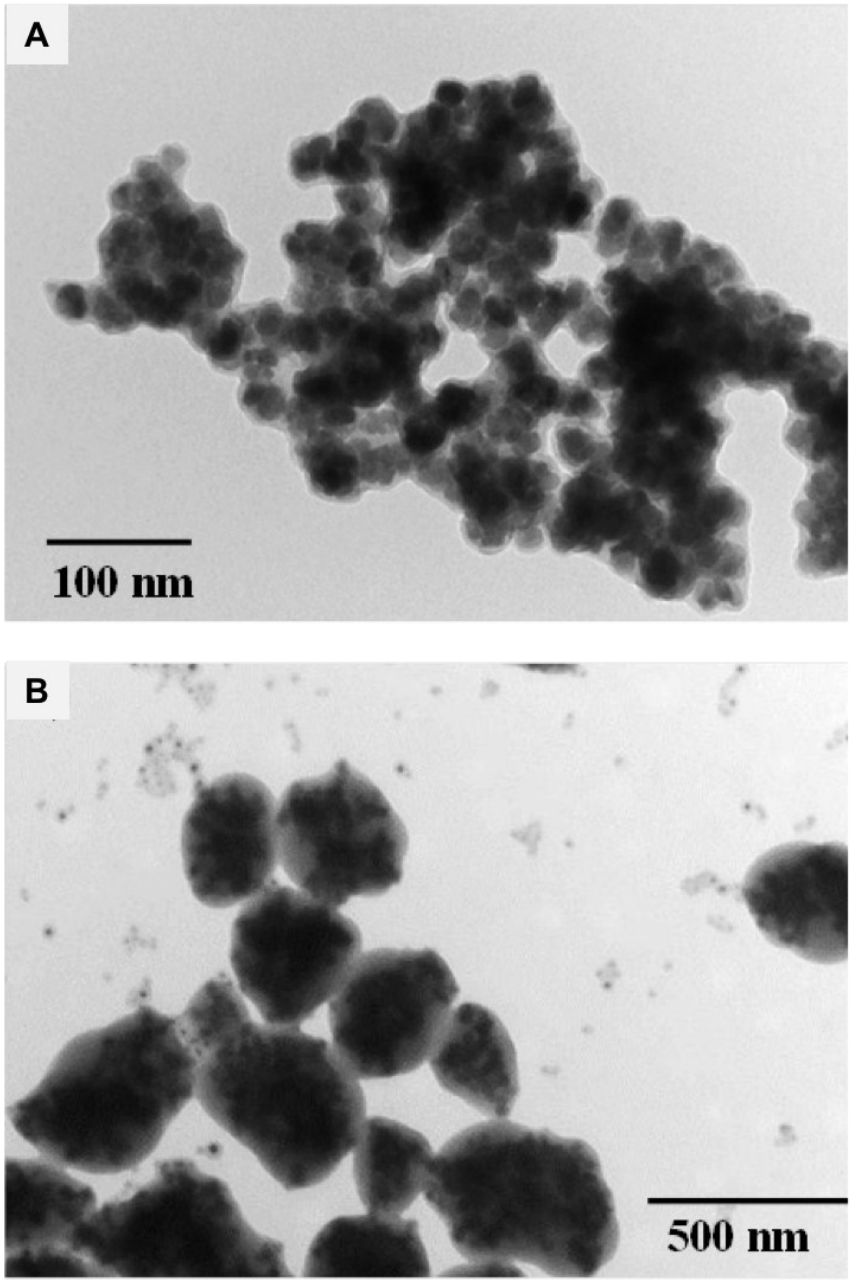

Fig. S3. TEM images of Au/Fe_3O_4@polymer NPs for A) 6 μL and B) 10 μL hydrothermal reactions including 200 ppm of carboxylate-coated Fe_3O_4 NPs. To understand the formation of the Fe_3O_4-involving Au/Fe_3O_4@polymer NPs, we used a magnet to collect the samples.

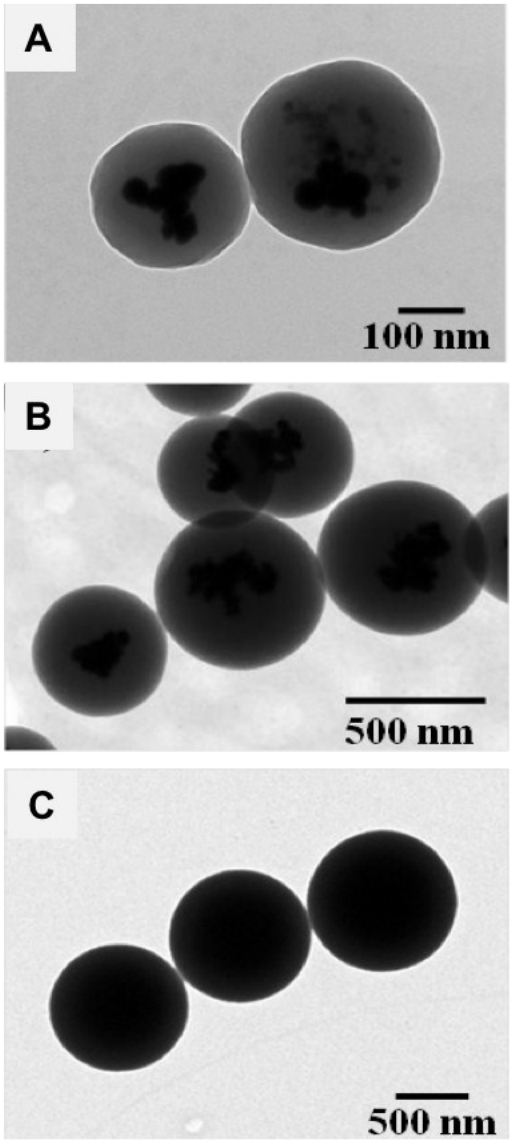

Fig. S4. TEM images of the Au/Fe_3O_4@polymer NPs for A) 22 μL, B) 30 μL, and C) 35 μL hydrothermal reactions with 200 ppm of carboxylate-coated Fe_3O_4 NPs. The particle size of as-prepared Au/Fe_3O_4@polymer NPs increased with an increment of the HCl concentrations.

To understand the composite formation mechanism, time-dependent TEM images (Fig. S5) were collected to investigate the assembly process of the PSMA polymer, Au species, and Fe_3O_4 NPs during the formation of the Au-Fe_3O_4@PSMA nanocomposites. At a reaction time of 1 h, the colloidal Fe_3O_4 particles were clustered. The particle surfaces were

observed to be covered with a thin polymer layer (i.e., PSMA). Hydrogen bonding interactions between the carboxylic acids of the PSMA polymer and the carboxylic groups on the surfaces of the Fe_3O_4 NPs were suggested because protonation of the COO^- groups occurred under acidic conditions. Meanwhile, some Au nanocrystals were formed on the outermost surface of the Fe_3O_4 NPs. When the reaction time was extended to 2 h, polyhedral Au NPs (triangles, pentagons, and hexagons) were obtained. Notably, each Au NP also had a thin polymer coating. Numerous free polymer NPs were produced as well. The addition of Fe_3O_4 NPs did not interfere with the reduction of $HAuCl_4$ by the oxidation of PSMA. As the reaction continued, we observed that free polymer NPs, small Au@polymer nanocomposites, and clustered Fe_3O_4 NPs began to fuse together at 6 h. The spherical Au NPs grew into large ones between 6 and 13 h of reaction time. In the acid system, several unstable Au nanocrystals were potentially dissolved into Au species and then grown on the bigger ones again, favoring thermodynamic stability.

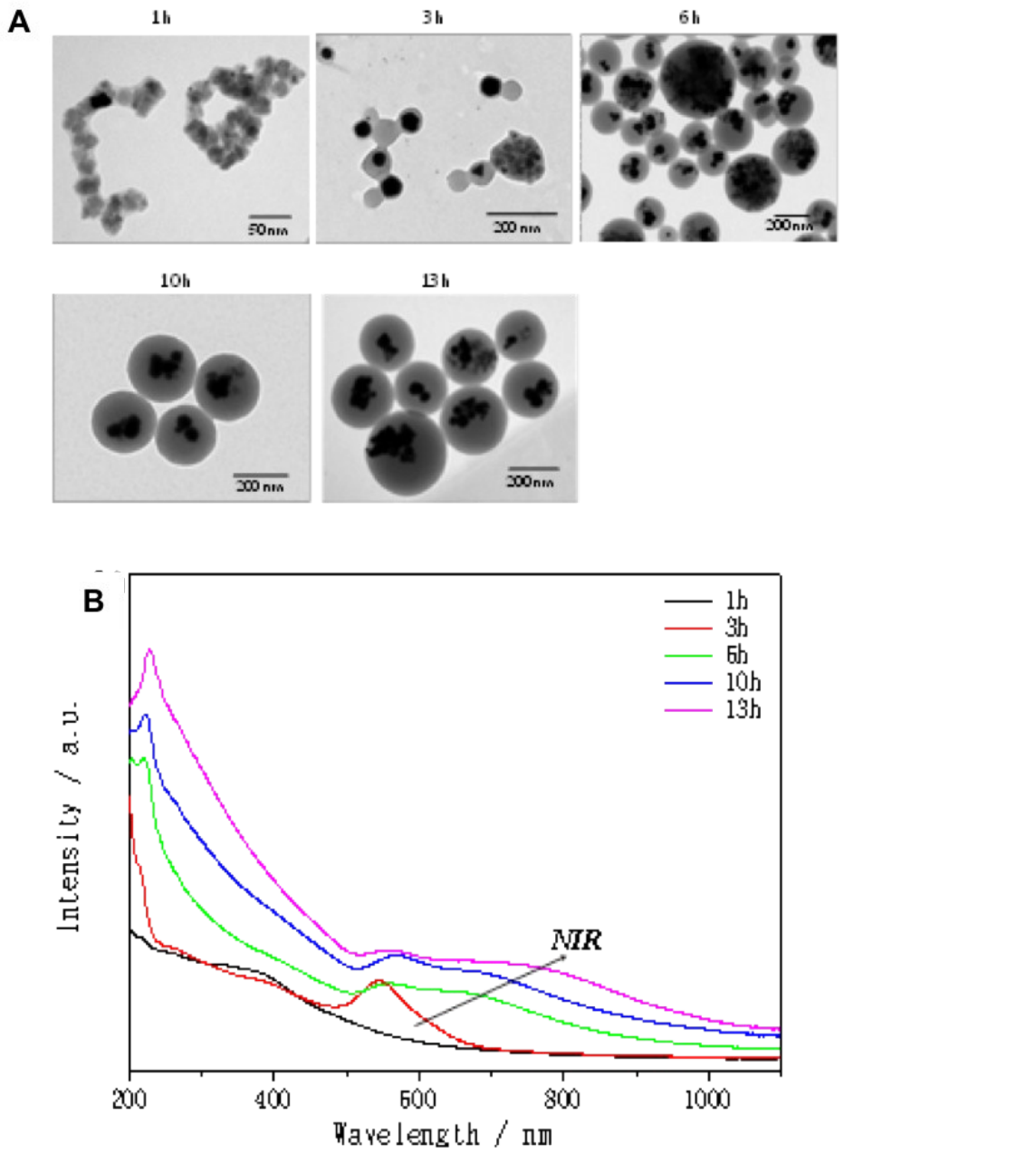

Fig. S5. Time-dependent A) TEM images and B) UV-visible spectra for monitoring the formation of Au/carboxylate-coated Fe_3O_4@polymer NPs in a mixture of18 μL of HCl and 200 μL of Fe_3O_4 NPs. To understand the formation process and not miss any information, we did not use a magnet to collect of the Fe_3O_4-containing Au/carboxylate-coated Fe_3O_4@polymer nanoparticles. After centrifugation at 500 rpm for 2 min, the samples were directly subjected to TEM for observation.

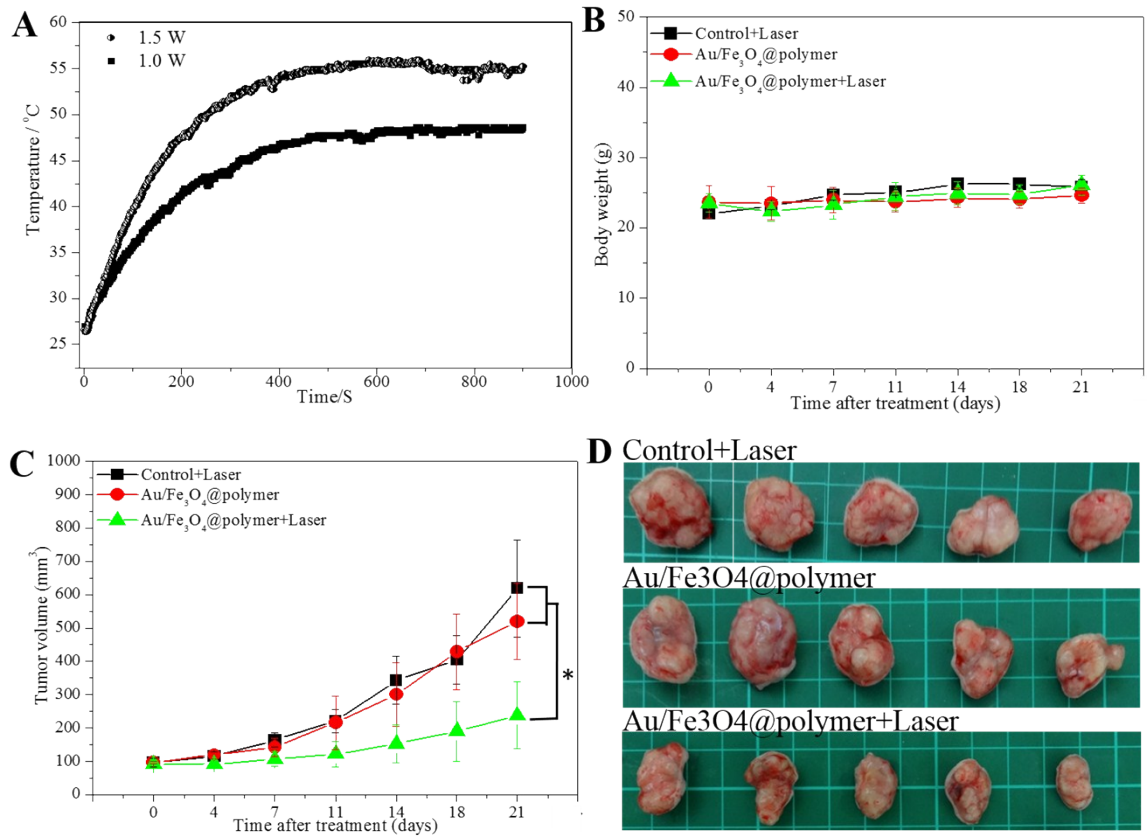

Fig. S6 A) Temperature dependence of NIR-irradiated Au/Fe_3O_4@polymer NPs (500 $ppm_{[Au]}$) solution as a function of irradiation time at a power density of 1.5 W/cm^{-2} and 1.0 Wcm^{-2}. B), C) and D) Antitumor effect of contorl+laser, Au/Fe_3O_4@polymer NPs, and Au/Fe_3O_4@polymer NPs+laser in HT29 tumor-bearing athymic nude mice. * significantly different compared with the control group (ANOVA, * $p \leqq 0.05$).

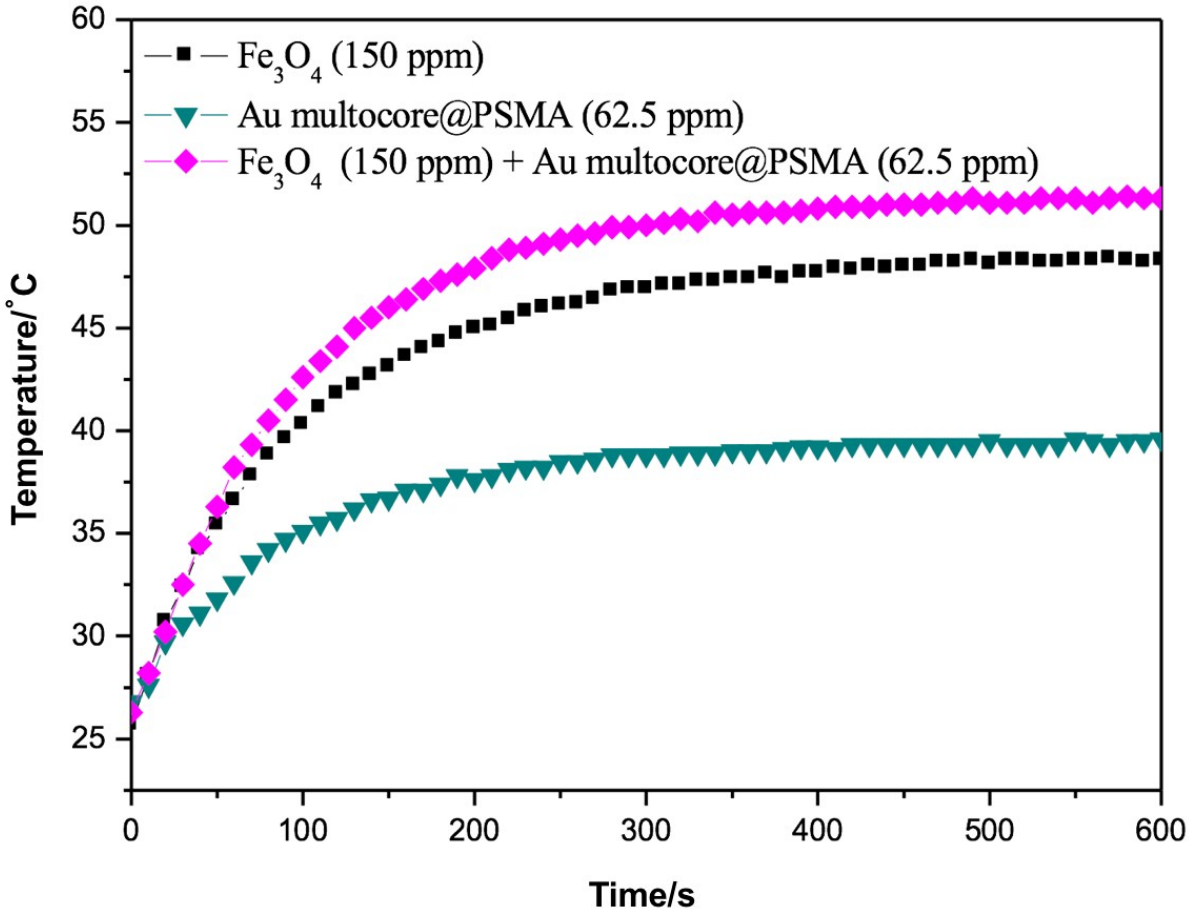

Fig. S7. Temperature dependence of the 0.1 mL Fe_3O_4 nanoparticles (150 ppm), Au multicore@PSMA (62.5 ppm), and a mixture solution including Fe_3O_4 nanoparticles (150 ppm) and Au multicore@PSMA (62.5 ppm) as a function of irradiation time at 808 nm (1.5 W/cm^2). This result verified the improvement of the photothermal effect with the addition of Fe_3O_4 nanoparticles into the Au multicore@PSMA solution.

The loading amount was determined to be ~190 mg/g based on UV-visible absorption measurements (Fig. S9). The FTIR spectrum of DOX binding onto the surfaces of the Au/Fe_3O_4@polymer NPs was acquired by employing ultra-high spatial resolution SR-IMS (Fig. S10). The result of Zeta-potential measurements revealed that the presence of a high density carboxylic acid groups binding onto the nanocomposite surface ascribed to negative charge of -35.2 mV of the Au/ Fe_3O_4@polymer NPs. Specially, the surface structure of PSMA also consisted of a polystyrene portion with C=C bonds. Strong mid-infrared absorption of DOX molecules binding onto the Au/Fe_3O_4@polymer NPs was attributed to a cooperative effect of electrostatic force and π-π interactions between the organic sheath of the nanocarrier and the DOX molecules. Consequently, the surface of the Au/ Fe3O4@polymer NPs has an advantage for multiplex interactions with positively charged and π-characterized molecules (i.e., DOX anticancer drug). On the contrary, for a negative charge π-characterized FITC molecule the loading efficiency was approximately 3 times lower.

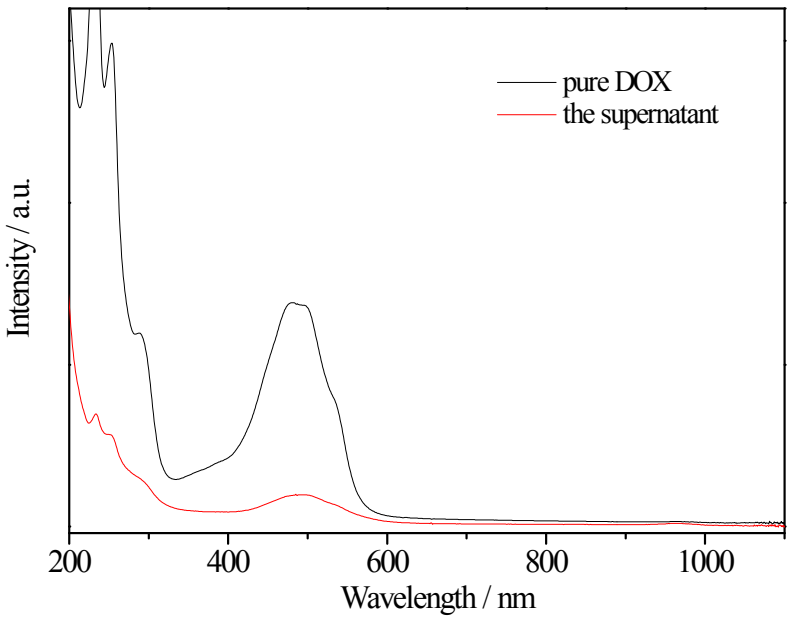

Fig. S8. UV-visible spectra recorded for free DOX (76.5 μM) and the remaining free DOX in the supernatant after the absorption of DOX (76.5 μM) onto the Au/Fe_3O_4@polymer NPs.

Synchrotron-based infrared microspectroscopy (SR-IMS) can achieve ultra-high spatial resolution approaching the diffraction limit and can be used in a number of biologically

relevant measurement techniques. The FTIR spectra of Au/Fe_3O_4@polymer-DOX NPs and pure DOX were acquired using SR-IMS. The spectrum of pure DOX has been previously reported.[1,2] The detailed characteristic absorptions and vibration motion assignments for the FTIR spectra of DOX and the Au/Fe_3O_4@polymer-DOX NPs are shown in Fig. S10. In this study, the FTIR spectrum of pure DOX showed that absorption bands were observed at 3467 cm^{-1}, 3367 cm^{-1}, 1615 cm^{-1}, and 1580 cm^{-1}, assigned to νs O-H stretching vibration, a doublet of νs N-H stretching, and bending vibrations, respectively. The characteristic absorption bands of the alkyl group of DOX were observed at 2977 cm^{-1}(ν_{as} asymmetric stretching vibration of CH_3), 2938 cm^{-1} (ν_{as} asymmetric stretching of CH_2), and 2845 cm^{-1} (ν_s symmetric stretching of CH_2). Other absorption bands were also observed at 1722 cm^{-1}, 1409 cm^{-1}, and 1283 cm^{-1}, assigned to ν_s C=O stretching vibrations, δ O-H…O deformation of the phenyl skeleton and ν C-O-H bending vibrations, respectively. For the Au/ Fe_3O_4@polymer-DOX nanocarriers, the absorption bands at 3061 cm^{-1}, 1713 cm^{-1}, 1600 cm^{-1} and 1578 cm^{-1} were attributed to ν C=CH stretching vibrations, ν_s C=O stretching vibrations and a doublet of δ NH_2 bending vibrations, respectively. The broad band observed at 3168 cm^{-1} was assigned to hydrogen bonded ν_s O-H stretching vibrations. The bands of the alkyl group were observed at 2920 cm^{-1}, 2852 cm^{-1}, 1493 cm^{-1}, 1450 cm^{-1}, and 1397 cm^{-1} and were assigned to as CH_2 asymmetric stretching vibrations, ν_s CH_2 symmetric stretching vibrations, aromatic C-C stretching vibrations, δ CH_2 bending vibrations and δ CH_3 bending vibrations, respectively. In this data, we also observed that, compared to pure DOX, the intensity of the N-H vibration signal of the Au/Fe_3O_4@polymer-DOX NPs was reduced because of DOX attachment to the Au/Fe_3O_4@polymer NPs via π-π stacking-mediated adsorption. The increase in the vibration signal for C-H was attributed to the sp^3 C-H bonds of PSMA. On the basis of these findings, the FTIR results revealed that the

attachment of DOX encapsulated within Au/Fe_3O_4 nanoparticles occurred via interactions of the -NH_2 and -OH groups of DOX.

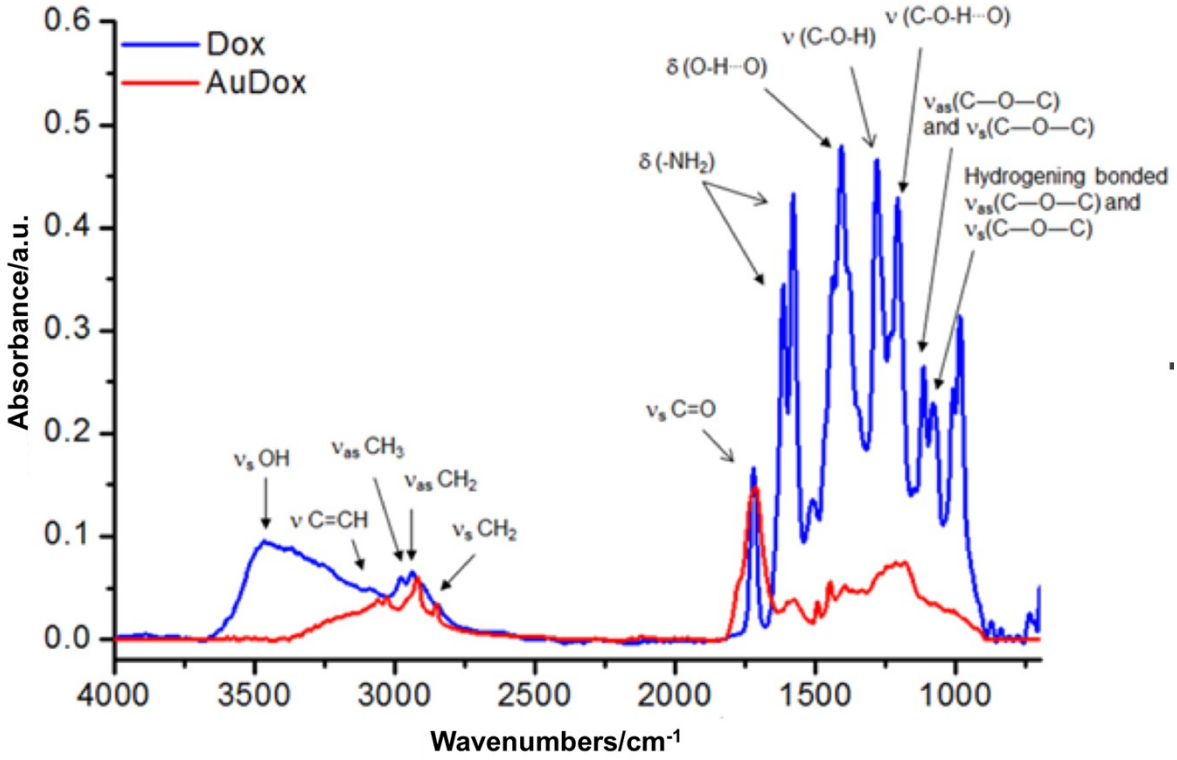

Fig. S9. FTIR spectra of pure DOX and Au/Fe_3O_4@polymer-DOX NPs.

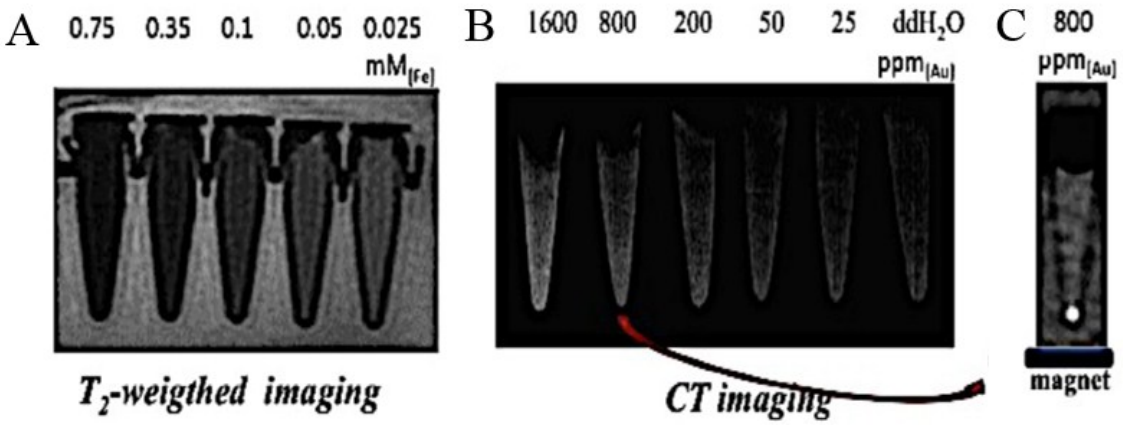

Fig. S10. A) T_2-weighted images and B) CT images of Au/Fe_3O_4@polymer NPs as a function of Fe and Au concentrations, respectively. C) CT imaging to monitor magnetic guided move to draw Au/Fe_3O_4@polymer NPs to bottom.

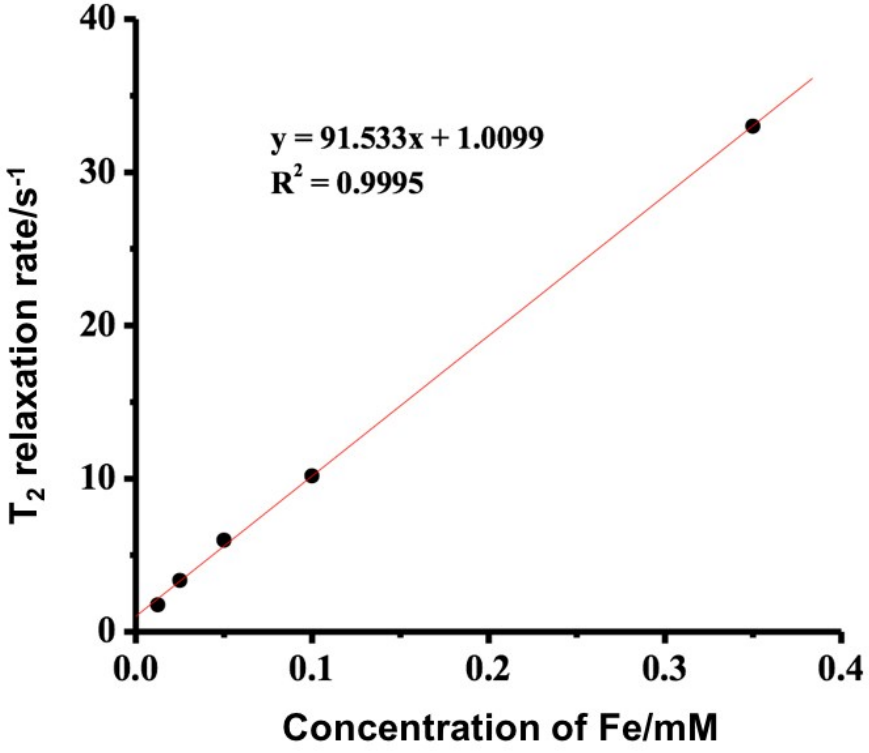

Fig. S11. T_2 relaxation ($1/T_1$, s^{-1}) rate of Au/carboxylate-coated Fe_3O_4@polymer NPs as a function of the iron concentration (mM).

References:

1. S. Kayal, R. V. Ramanujan, *Mater. Sci. Eng. C.,* **2010**, 30, 484-490
2. C.J. Lee, J. S. Kang, M.S. Kim, K.P. Lee, M.S. Lee, Bull. Korean Chem. Soc., 2004, 25, 1211-1216.